

A generalized analysis of capillary flows in channels

Yan Xiao, Fuzheng Yang, Ranga Pitchumani *

Advanced Materials and Technologies Laboratory, Department of Mechanical Engineering, University of Connecticut, Storrs, CT 06269-3139, USA

Received 29 August 2005; accepted 5 January 2006

Available online 15 February 2006

Abstract

Investigations on the motion of a fluid in capillary geometries have been extensively reported in the literature using both experimental and theoretical approaches. In this paper, the theories for capillary flow are generalized to a unified nonlinear second-order differential equation which takes the effects of the entrance, the inertial forces, and the dynamic contact angle into account. An analytical solution of the differential equation is obtained in the form of a double Dirichlet series. The readily evaluated analytical solution is compared with experimental and numerical results in the literature, which shows a good agreement. It is demonstrated that this analytical approach can be used to predict capillary flows for a wide range of fluids and parallel-plate and tube geometries in a unified manner.

© 2006 Elsevier Inc. All rights reserved.

Keywords: Capillary flow; Dynamic contact angle; Analytical model; Minichannels; Tube; Parallel plates

1. Introduction

Research on capillary-driven flows, dating its origin back to more than one century ago, is still a subject of interest due to the widespread applications in materials manufacturing, oil production, ink printing, and transportation of propellant, among other modern engineering fields [1–3]. For a fully developed capillary driven flow, the analysis on the balance of viscous force, surface tension force, and gravitational force yields the classical Washburn equation on the penetration depth, h , evolution with time, t [4]. While this analysis holds for describing the long-time capillary flow behavior, it does not account for several forces that prevail in the initial stages of a capillary flow process.

Several modifications to the Washburn equation have been reported to include the inertial force and entrance pressure loss effects [3,5–10]. A simple method to incorporate the entrance pressure loss was adopted in Ref. [5] by evaluating the energy loss using an empirical energy loss coefficient. Duarte et al. [6] employed a hydrodynamical approach by averaging the Navier–Stokes equation along the liquid column in the capillary geometry, and the velocity variation at the entrance was

taken into consideration. In this approach, the details of the liquid motion in the vicinity of the flow front are neglected, and the obtained equation is not applicable to the initial time $t = 0$. A more elaborate approach considered the motion of the fluid in a wider region of the flow field, including the fluids both in the capillary tube and in the fluid reservoir [1,2,7–10].

Most studies on capillary flows assumed constant contact angle between the advancing liquid front and the solid wall; however, experimental observations have shown a strong dependence of the contact angle on the velocity of the meniscus (flow front) movement [11–13]. Several empirical relations are available to describe the dynamic contact angle as a function of time [14–17]. The Hoffman function [14] can be applied to the case of capillary flow in horizontal channels where the effects of the inertial force and gravity are negligible. Bracke and Sciffer relations [15,16] are not applicable to the case when the dynamic contact angle starts with an initial value of 90° and gradually approaches the equilibrium value. The Newman model [17] may be applied to all types of capillary flows; however, a fitting parameter in the model must be determined from experimental data.

Based on the different considerations of inertial force, entrance effect, and dynamic contact angle mentioned above, a set of nonlinear first- or second-order differential equations were derived in the literature [1–10]. The majority of the studies

* Corresponding author. Fax: +1 860 486 5088.
E-mail address: pitchu@engr.uconn.edu (R. Pitchumani).

solved the governing equations using a numerical method, and to the knowledge of the authors, analytical solutions were obtained only for several specific cases of capillary flows [1,6,18]. Zhmud [1] presented two asymptotic solutions for the time to approach zero and infinity, respectively. Duarte et al. [6] linearized the differential equation and reported a perturbation solution for the capillary flow in a tube. Brittin [18] developed an analytical approach using a double Dirichlet series for the motion of the liquid in a capillary tube, where the contact angle is assumed to be constant. The principal limitations of the available analytical analyses lie in the fact that the results are only applicable to specific geometry and constant contact angles. Furthermore, the principle of superposition (valid only for linear systems) was inappropriately employed by Barraza et al. [3] for the capillary flow between parallel plates, which is governed by a nonlinear differential equation.

An objective of the paper is to present a generalized description of capillary flows in a range of geometries and configurations encountered in engineering practice. A generalized nonlinear second-order differential equation is derived, and solved analytically to obtain readily usable solutions applicable to different geometries and time varying contact angles. The development of the general theory for capillary flows in parallel-plate and tube geometries is presented in Section 2, followed by the analytical approach for solving the governing equation in Section 3. Section 4 demonstrates the validation of the theory via comparison of the analytical solution to numerical results and experimental data available in the literature.

2. Mathematical model for capillary flows

A generalized theoretical model is developed for capillary flows in two types of commonly adopted geometries, namely, (1) parallel plates and (2) tubes. In Figs. 1a and 1b, a pair of parallel plates with a gap spacing $2B$ and width $2W$ is positioned perpendicular to a horizontal liquid surface in the x – y plane. The origin of the Cartesian coordinate system is located on the flat liquid surface and the center of the gap. Owing to the surface tension and the adhesion of liquid molecules to the solid wall, a three-dimensional saddle-shaped meniscus forms at the liquid/air interface. The travel length of the liquid along the z -axis is referred to as the penetration depth h , which is measured from the origin to the valley (or peak) point of the meniscus in Fig. 1a (or Fig. 1b). Note that the radii of curvature of the meniscus in the x – z and y – z planes are represented by R_1 and R_2 , respectively. Fig. 1c presents a schematic of the capillary-driven flow in a vertical tube of radius r_0 , in which the meniscus assumes a paraboloid shape due to the axisymmetry of the geometry. The origin of the cylindrical coordinate system corresponds to the intersection between the tube axis and the horizontal liquid surface, and the penetration depth is defined as the distance from the origin to the valley point of the paraboloid. The portions of liquid marked by the dashed lines in Figs. 1a–1c denote control volumes, which are employed to derive the equation for the dynamics of the capillary driven flow with time, t .

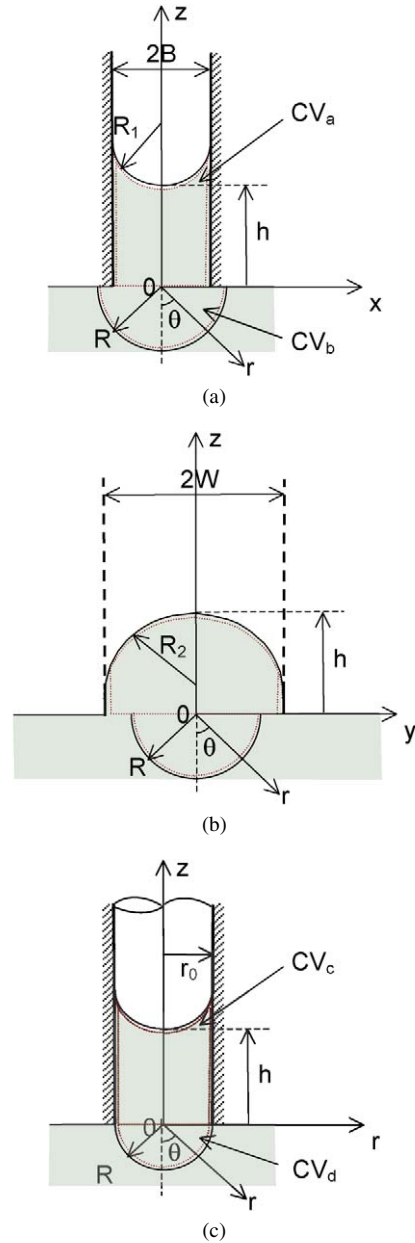


Fig. 1. Schematic of two capillary geometries: (a) and (b) parallel plates; (c) tube. The geometric parameters and the coordinate systems are identified in the figure.

The model development is based on the conservation of mass and linear momentum, subject to the assumptions that the liquid is incompressible, homogeneous, and Newtonian. Considering a deformable control volume (CV_a) encompassing the penetrated region between the two parallel plates in Fig. 1a, the integral momentum equation in the z -direction may be written as [2]

$$\sum F_z = \frac{\partial}{\partial t} \left[\int_0^h \int_{-W}^W \int_{-B}^B \rho v_z dx dy dz \right] + \int_{-W}^W \int_{-B}^B v_z (-\rho v_z) dx dy, \quad (1)$$

where $\sum F_z$ denotes the sum of forces acting on the control volume in the z -direction, ρ is the density of the liquid, v_z represents the velocity of the fluid in the z -direction within the control volume, and the detailed profile of the meniscus is neglected in the above formulation. In order to evaluate the two terms on the right-hand side of Eq. (1), the information on the velocity profile between the plates is required. Since the flow between the plates is laminar in nature, a fully developed flow with parabolic profile for the velocity v_z may be used to approximate it, that is, the deviations from the parabolic velocity distribution in the entrance region and at the flow front are ignored [2]

$$v_z = \frac{3}{2} \frac{dh}{dt} \left[1 - \left(\frac{x}{B} \right)^2 \right], \quad (2)$$

where $\frac{dh}{dt}$ is the rate of progression of the flow front. Note that since the gap between the plates, $2B$, is usually much smaller than the plate width, $2W$, the fully developed velocity profile is considered to be uniform along the width while varying in the gap-wise (x -) direction only. This assumption is generally valid except for a region near the edges ($y \approx \pm W$). The use of a fully developed velocity profile in the analysis constitutes an approximation, whose accuracy will be limited in regions near the entrance and the flow front. Since the spontaneous capillary flow is laminar in nature with Reynolds number much less than 50, the entrance length evaluates to about twice the hydraulic diameter of the channel [6]. The meniscus depth is also very small. Since the regions of entrance and the flow front are both small, the error introduced by the approximation is restricted to a very short time near zero, but otherwise reasonably accurate over the range of the capillary flow times considered in the studies.

Four forces acting on the control volume may be identified, namely, the viscous force, F_v , along the solid wall, the pressure force at the flow front, F_{pf} , the pressure force at the inlet to the parallel plates, F_{pi} , and the gravity force, $F_g = -4BW\rho gh$. By assuming the fully developed velocity profile in Eq. (2), the viscous force, F_v , is readily obtained as [2]

$$F_v = 2 \int_0^h \int_{-W}^W \left(\mu \frac{dv_z}{dx} \right)_{x=\pm B} dy dz = -12\mu h \frac{W}{B} \frac{dh}{dt}, \quad (3)$$

where μ is the viscosity of the liquid. The pressure force at the flow front is governed by the Young–Laplace equation, which, in turn, is derived via the force balance among the liquid pressure, surface tension, and ambient pressure [2]

$$\begin{aligned} F_{pf} &= \int_{-W}^W \int_{-B}^B \left[\sigma \left(\frac{1}{R_1} + \frac{1}{R_2} \right) - p_0 \right] dx dy \\ &= 4BW \left[\sigma \left(\frac{\cos \theta_d}{B} - \frac{1}{W} \right) - p_0 \right], \end{aligned} \quad (4)$$

where σ is the surface tension of the liquid in contact with air, θ_d denotes the *dynamic* contact angle between the liquid and the solid surfaces, and p_0 is the atmospheric pressure. An accurate

calculation of F_{pf} requires the three-dimensional topography of the meniscus surface. In Eq. (4), the major radii of curvature of the liquid/air interface are simplified to be: $R_1 = B/\cos \theta_d$ and $R_2 = -W$ [2]. The negative sign for R_2 implies that the curvature in y - z plane acts to retard the liquid motion. Studies in the literature reveal that the *dynamic* contact angle is governed by a relaxational spreading process, gradually developing from an initial value of 90° to the equilibrium value θ_e [17]. The time evolution of θ_d is commonly described by the Newman relationship as follows [10]

$$\cos \theta_d = \cos \theta_e [1 - \exp(-\sigma t / \mu M)], \quad (5)$$

where M is an empirical constant specific to the combination of fluid and solid surface in contact, and is interpreted as the characteristic distance over which the spreading takes place.

The pressure force, F_{pi} , is obtained as an integral of the pressure at the inlet to the channel, $p(x, y, 0)$, across the channel cross section as follows

$$F_{pi} = - \int_{-W}^W \int_{-B}^B p(x, y, 0) dx dy. \quad (6)$$

Evidently, the three-dimensional flow field near the entrance must be solved to accurately determine the distribution of the inlet pressure $p(x, y, 0)$. An approximation of $p(x, y, 0)$ is obtained by considering the integral momentum balance to a hemispherical control volume denoted as CV_b in Figs. 1a and 1b in the liquid reservoir below the parallel plates, such that outside CV_b in the reservoir, the velocity distribution is that of a sink flow. The diametral cross section of CV_b adjoins the entrance plane of the parallel plates, and the diameter is determined by equating the projected cross-sectional area to that of the gap between the parallel plates (i.e., $4BW$). Following similar analyses in Refs. [2] and [7], the inlet pressure is obtained as



$$\begin{aligned} p(x, y, 0) &= p_0 - \left[1.11\rho\sqrt{BW} \frac{d^2h}{dt^2} + 1.158\rho \left(\frac{dh}{dt} \right)^2 \right. \\ &\quad \left. + \frac{1.772\mu}{\sqrt{BW}} \frac{dh}{dt} \right]. \end{aligned} \quad (7)$$

Note that the constants in Eq. (7) result from the analysis, and are not empirical values. Furthermore, the inlet pressure $p(x, y, 0)$ is less than the ambient pressure owing to the effects of entrance losses and the inertia of the fluid flowing into the gap.

In Eq. (1), the sum of forces on the left-hand side may be determined by employing Eqs. (3)–(7), and the two terms on the right-hand side are readily evaluated using the velocity profile in Eq. (2); the resulting equation for the time evolution of the penetration depth, $h(t)$, is obtained as [2]

$$\begin{aligned} &\left(h + 1.11\sqrt{BW} \right) \frac{d^2h}{dt^2} + 0.958 \left(\frac{dh}{dt} \right)^2 \\ &+ \left(\frac{3\mu}{\rho B^2} h + \frac{1.772\mu}{\rho\sqrt{BW}} \right) \frac{dh}{dt} + gh - \frac{\sigma}{\rho} \left(\frac{\cos \theta_d}{B} - \frac{1}{W} \right) = 0. \end{aligned} \quad (8)$$

Table 1
Constants in Eq. (9)

| Geometry | Schematic | c_1 | c_2 | c_3 | c_4 | c_5 | c_6 |
|-----------------|---|-------------------------------|-------|-------|----------------------|----------------------|--|
| Parallel plates |  | $\frac{0.555}{\sqrt{\gamma}}$ | 0.958 | 1 | $0.295\sqrt{\gamma}$ | $\frac{Bo}{144Oh^2}$ | $\frac{\gamma - \cos\theta_d}{72Oh^2}$ |
| Tube |  | 1.028 | 0.958 | 1 | 0.25 | $\frac{Bo}{64Oh^2}$ | $\frac{-\cos\theta_d}{32Oh^2}$ |

The penetration depth evolution in capillary tubes may be similarly derived by applying the integral analysis to the cylindrical and hemispherical control volumes, CV_c and CV_d , in Fig. 1c, respectively. For CV_c a version of Eq. (1) in the cylindrical coordinates applies, with the following expression for the axial velocity profile, v_z [7]

$$v_z = 2 \frac{dh}{dt} \left[1 - \left(\frac{r}{r_0} \right)^2 \right].$$

Note that the four external forces on CV_a also exist on CV_c , and the integral momentum equation for CV_d follows that of the control volume CV_b . The detailed model development for capillary tubes is omitted in this section for the purpose of brevity, and is left as an exercise for the interested readers.

To facilitate easier physical interpretation, a dimensionless equation for the penetration depth evolution in parallel plates and capillary tubes is derived by introducing the following dimensionless time, t^* , and penetration depth, h^*

$$t^* = \frac{t}{t_0}, \quad h^* = \frac{h}{h_0},$$

where the characteristic time t_0 and length h_0 are defined as: $t_0 = \frac{\rho(2B)^2}{12\mu}$, $h_0 = 2B$ for the parallel plates, and $t_0 = \frac{\rho r_0^2}{8\mu}$, $h_0 = r_0$ for the capillary tubes. Using these definitions, a generalized dimensionless equation for the penetration depth evolution in both parallel plates and tubes is obtained as

$$(h^* + c_1) \frac{d^2 h^*}{dt^{*2}} + c_2 \left(\frac{dh^*}{dt^*} \right)^2 (c_3 h^* + c_4) \frac{dh^*}{dt^*} + c_5 h^* + c_6 = 0, \quad (9)$$

where the constants c_1 – c_6 are tabulated in Table 1. For the case of parallel plates, the dimensionless groups involved in the constants are (1) the aspect ratio $\gamma = \frac{B}{W}$, (2) the Ohnesorge number representing the ratio of viscous force to surface tension force $Oh = \frac{\mu}{\sqrt{2B\rho\sigma}}$, and (3) the Bond number denoting the ratio of gravity force to surface tension force $Bo = \frac{\rho g(2B)^2}{\sigma}$; two dimensionless groups are identified for the case of capillary tubes, namely, $Oh = \frac{\mu}{\sqrt{r_0\rho\sigma}}$, and $Bo = \frac{\rho g r_0^2}{\sigma}$. The initial conditions for Eq. (9) are zero penetration depth and velocity for the flow front, namely,

$$h^*(0) = 0, \quad \frac{dh^*}{dt^*}(0) = 0. \quad (10)$$

3. Analytical solution

Equation (9) and associated initial conditions are solved using a double series solution approach reported in Ref. [18]. Note

that the coefficient c_6 represents the effect of dynamic contact angle, which, in turn, may be time-dependent. The analytical solution for the case of constant contact angle is first obtained, and is subsequently extended to the case of time-varying contact angle. Following the technique in Ref. [18], the dimensionless penetration depth, h^* , is represented by a function series

$$h^* = \sum_{i=0}^{\infty} \phi_i(t^*) \lambda^i, \quad (11)$$

where λ is an arbitrary parameter independent of t^* , and the functions $\phi_i(t^*)$ are determined in the following. Substituting Eq. (11) into Eq. (9) yields

$$\sum_{i=0}^{\infty} (\alpha_i + c_1 \phi_i'' + c_2 \beta_i + c_3 \gamma_i + c_4 \phi_i' + c_5 \phi_i) \lambda^i + c_6 = 0, \quad (12)$$

where

$$\alpha_i = \sum_{k=0}^i \phi_k \phi_{i-k}'', \quad \beta_i = \sum_{k=0}^i \phi_k' \phi_{i-k}', \quad \gamma_i = \sum_{k=0}^i \phi_k \phi_{i-k}',$$

and primes represent derivatives with respect to time. The coefficient of each λ^i in Eq. (12) must be zero since λ is arbitrary, and a set of differential equations is obtained for the $\phi_i(t)$.

$$(\phi_0 + c_1) \phi_0'' + (c_2 \phi_0' + c_3 \phi_0 + c_4) \phi_0' + c_5 \phi_0 + c_6 = 0, \\ \alpha_i + c_1 \phi_i'' + c_2 \beta_i + c_3 \gamma_i + c_4 \phi_i' + c_5 \phi_i = 0, \quad i > 0. \quad (13)$$

A particular solution for ϕ_0 has the form

$$\phi_0 = -c_6/c_5. \quad (14)$$

Substituting the solution in Eq. (14) into Eq. (13), the following differential equation for ϕ_i , $i > 0$ is obtained

$$(\phi_0 + c_1) \phi_i'' + (c_3 \phi_0 + c_4) \phi_i' + c_5 \phi_i \\ = - \sum_{k=1}^{i-1} [\phi_k \phi_{i-k}'' + c_2 \phi_k' \phi_{i-k}' + c_3 \phi_k \phi_{i-k}'] = F_i(t^*). \quad (15)$$

The general solution of Eq. (15) is [18]:

$$\phi_i(t^*) = C_i \exp(r_1 t^*) + D_i \exp(r_2 t^*) \\ + \int_0^{t^*} G(t^* - \tau) F_i(\tau) d\tau, \quad (16)$$

where C_i and D_i are arbitrary constants, r_1 and r_2 are the roots of the characteristic equation

$$(\phi_0 + c_1)r^2 + (c_3 \phi_0 + c_4)r + c_5 = 0, \quad (17)$$

and the function $G(t^*)$ is given by

$$G(t^*) = \frac{1}{r_2 - r_1} [\exp(r_1 t^*) - \exp(r_2 t^*)].$$

For most liquid flows in capillary geometries, the roots r_1 and r_2 are distinct, real, and negative [18].

It must be mentioned that the evaluation of the integral $\int_0^{t^*} G(t^* - \tau) F_i(\tau) d\tau$ results in terms of the type $\exp(mr_1 t^*) \times \exp(nr_2 t^*)$, where m and n are integers [18]. Substituting

Eq. (16) into Eq. (11) and setting $\lambda = 1$, a double Dirichlet series is obtained to represent the solution of Eq. (9) with constant contact angle

$$h^* = \sum_{m=0}^{\infty} \sum_{n=0}^{\infty} a_{m,n} \exp[(mr_1 + nr_2)t^*], \quad (18)$$

where the coefficients $a_{m,n}$ may be determined by substituting Eq. (18) into the differential equation (9), and equating the coefficients before the exponential terms $\exp[(mr_1 + nr_2)t^*]$ to be zero. The coefficient $a_{0,0}$ is evaluated to be $-c_6/c_5$ (i.e., ϕ_0), and a recursive relation is obtained for the other coefficients in the series

$$\begin{aligned} a_{m,n} = & \left[\sum_{k=0}^m \sum_{l=0}^n a_{k,l} a_{m-k,n-l} \left\{ (kr_1 + lr_2)^2 (1 - c_2) \right. \right. \\ & \left. \left. + (kr_1 + lr_2) [c_2(mr_1 + nr_2) + c_3] \right\} \right] \\ & \times [(a_{0,0} + c_1)(mr_1 + nr_2)^2 \\ & + (c_3 a_{0,0} + c_4)(mr_1 + nr_2) + c_5]^{-1}, \end{aligned} \quad (19)$$

where the subscript pairs $(m, n) \neq (0, 0)$, $(0, 1)$, $(1, 0)$, and $(k, l) \neq (m, n)$. The two coefficients $a_{0,1}$ and $a_{1,0}$ may be determined from the two initial conditions as discussed below, and other coefficients in Eq. (18) are subsequently evaluated from Eq. (19).

As pointed out in Ref. [18] and observed for the capillary systems considered in this study, the two characteristic roots, r_1 and r_2 , are distinct for most capillary flows encountered in engineering practice. Considering r_1 to be of smaller magnitude of the two roots (i.e., $|r_1| < |r_2|$), a good approximation for the infinite series in Eq. (18) may be obtained by using only one term in r_2 and n_1 terms for r_1 [18]

$$h^* \approx a_{0,0} + a_{0,1} \exp(r_2 t^*) + \sum_{k=0}^{n_1} a_{k,0} \exp(kr_1 t^*). \quad (20)$$

Substituting Eq. (20) into the initial conditions, $h^*(0) = 0$ and $\frac{dh^*}{dt^*}(0) = 0$, two algebraic equations are obtained for the evaluation of $a_{0,1}$ and $a_{1,0}$

$$a_{0,0} + a_{0,1} + \sum_{k=0}^{n_1} a_{k,0} = 0, \quad (21)$$

$$a_{0,1}r_2 + \sum_{k=0}^{n_1} a_{k,0}(kr_1) = 0. \quad (22)$$

The elimination of $a_{0,1}$ between Eqs. (21) and (22) yields a polynomial equation of n_1 th degree in $a_{1,0}$

$$a_{0,0}r_2 + \sum_{k=0}^{n_1} a_{k,0}(r_2 - kr_1) = 0, \quad (23)$$

where $a_{k,0}$ can be evaluated by recursively applying Eq. (19). The real root of Eq. (23) with the smallest magnitude is taken as $a_{1,0}$, while the value of $a_{0,1}$ is obtained from Eq. (21). With the determination of the coefficients in the double series, Eq. (20)

may be used to predict the penetration depth evolution with time for capillary-driven flows with constant contact angle.

For the general case of time-varying dynamic contact angle, the temporal domain can be divided into several time intervals $(t_{i+1}^* - t_i^* = \Delta t_i^*)$, and $\cos \theta_d$ in each i th interval is considered to be constant with the average value between t_i^* and t_{i+1}^* , i.e., $(\int_{t_i^*}^{t_{i+1}^*} \cos \theta_d dt^*) / \Delta t_i^*$. Thus, the analytical solution in Eq. (20) may be employed to determine the time evolution of h^* in each i th time interval. It must be mentioned that the initial conditions for the i th time interval are obtained from the final values of h^* and $\frac{dh^*}{dt^*}$ in the previous time interval.

4. Results and discussion

The validation of the theoretical analysis is demonstrated in this section via comparison with experimental data and numerical results for capillary flows in the two geometries and for a wide range of fluids. The theoretical solutions are obtained by the evaluation of Eq. (20), while a fifth-order Runge–Kutta scheme [10] is adopted to solve Eq. (9) for numerical results. The fluid properties and geometries corresponding to the experimental data are summarized in the Table 2. The development of penetration depth, h^* , with time, t^* , is first discussed for capillary flows with constant contact angle in parallel plates, followed by a presentation on flows with dynamic contact angle in capillary tubes.

Fig. 2a shows the penetration process of ethanol between two vertical parallel plates with gap spacing $2B = 0.15$ mm and plates width $2W = 25$ mm. The symbols in the figure represent experimental data from Barraza et al. [3], the solid line denotes the numerical prediction, while the three dashed lines correspond to analytical solutions using different values of n_1 in Eq. (20). The penetration depth, h^* , increases quickly at the initial stage of the process, owing to relatively small resistances from gravity and viscous forces in the control volume CV_a (Fig. 1a). The resistances increase significantly with further liquid rise, while the driving capillary force (defined as the pressure difference between the inlet of the parallel plates and the flow front) remains relatively constant. Consequently, h^* approaches asymptotically an equilibrium value corresponding to the balance of the capillary and gravity forces. For the case of ethanol, the experimental result for the equilibrium contact angle is 20.1° , and the dynamic contact angle is assumed to be the same value, $\theta_d = \theta_e = 20.1^\circ$, in the numerical and analytical calculations, since the relaxation time to achieve θ_e is negligible compared to the total time for the capillary rise [3]. Evidently, the numerical prediction and the analytical solution with $n_1 = 20$ are in good agreement with the experimental data for the entire capillary-driven flow process. It is also seen that the accuracy of the analytical solution may be improved by increasing the number of terms, n_1 , in the double series, Eq. (20).

Following the format of Fig. 2a, Fig. 2b presents the capillary rise process for hexane in the same parallel plates configuration. Again, a constant contact angle $\theta_d = 32.7^\circ$, is adopted for the analytical and numerical computations due to short relaxation time of the hexane liquid in contact with the solid sur-

Table 2
Fluid properties and geometric parameters used in the analyses

| Fluid | Geometry | Dimensions [mm] | Density, ρ [kg/m ³] | Viscosity, μ [Pa s] | Surface tension, σ [N/m] | Equilibrium contact angle, θ_e [deg] |
|-------------------------------|--------------------|--------------------------|---|----------------------------|---------------------------------------|---|
| Ethanol [3] | Parallel plates | $2B = 0.15$ $2W = 25$ | 780.00 | 0.00117 | 0.0216 | 20.1 |
| Hexane [3] | Parallel plates | $2B = 0.15$ $2W = 25$ | 660.30 | 0.000326 | 0.0191 | 32.7 |
| Ethanol [12] | Tube | $r_0 = 0.295$ | 780.00 | 0.00117 | 0.0220 | 20.1 |
| Water [12] | Tube | $r_0 = 0.295$ | 998.20 | 0.001 | 0.0720 | 0 |
| Ethanol–water mixture [12] | Tube | $r_0 = 0.295$ | 980.64 | 0.001 | 0.0504 | 0 |
| PDMS oil 5 [13] | Tube | $r_0 = 0.315$ | 918.00 | 0.005 | 0.0197 | 0 |
| PDMS oil 10 [13] | Tube | $r_0 = 0.315$ | 935.00 | 0.01 | 0.0201 | 0 |

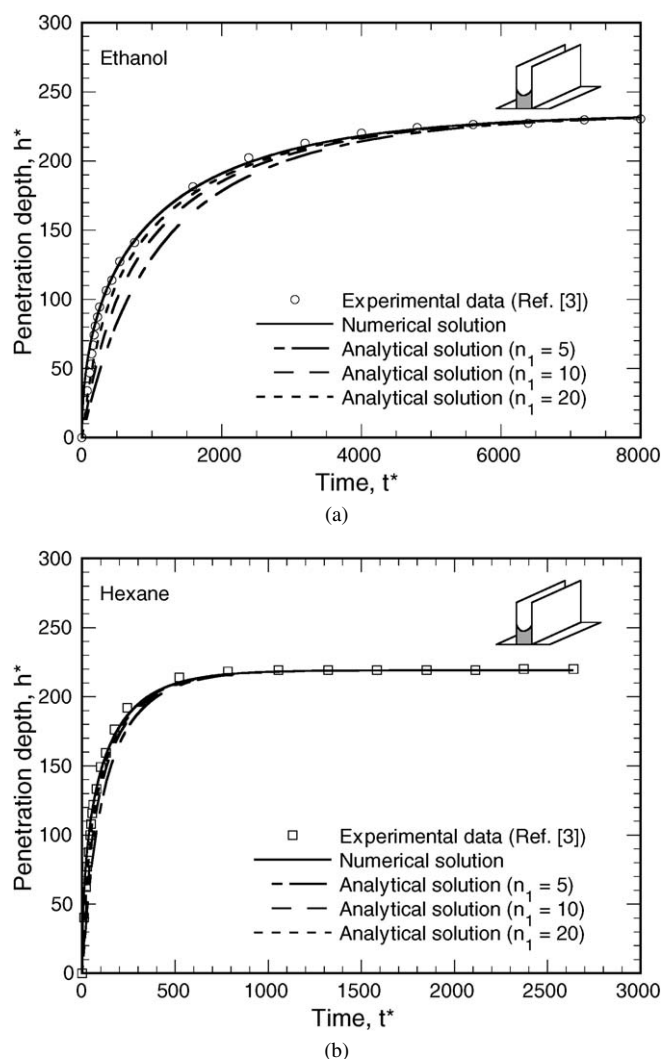


Fig. 2. Penetration depth as a function of time for the capillary flows of (a) ethanol and (b) hexane between two vertical parallel plates.

face, as reported in the literature [3]. It should be mentioned that the contact angle of 32.7° was obtained in Ref. [3] based on fitting their numerical simulation of capillary rise to the measured

data. An experimentally measured value of 11.8° obtained using the Wilhelmy plate technique is also reported in Ref. [3], but as stated in this reference, the lower value of the experimental data may be caused by hexane's vapor, which increases the saturation of the solid surface during the Wilhelmy plate experiment, while in the penetration experiment, the glass surface is completely dry [3]. This suggests that the measured equilibrium contact angle of 11.8° may not be appropriate for the description of the capillary rise of hexane between two dry parallel plates. The value of 32.7° is also consistent with the measured penetration depth of 33 mm [3] at the equilibrium state, when the capillary force is balanced by gravity. Based on these considerations, the constant contact angle of 32.7° is used, instead of 11.8° , for the calculations reported in Fig. 2b. Since the viscosity of hexane is about four times smaller than that of ethanol (see Table 2), the time for the hexane flow to rise to its equilibrium penetration depth is significantly reduced owing to the smaller viscous resistance. Note that the accuracy of the analytical series solution increases from $n_1 = 5$ to $n_1 = 20$, although the predictions are seen to be in close agreement with experimental data even for $n_1 = 5$.

With the validation of analysis on capillary flow with constant contact angle as basis, parametric studies on the capillary flows between two parallel plates are presented in Figs. 3a–3c; the solid lines represent the numerical predictions and the symbols denote the analytical solutions. A principal purpose of the parametric studies is to compare the analytical and numerical solutions in a wider parameter range not available in the experimental data. Fig. 3a presents the penetration depth, h^* , as a function of time, t^* , and aspect ratio, γ defined as the ratio of the gap to the plate width. The results correspond to the parameter combination of $Oh = 0.0075$, and $Bo = 0.0076$. When the aspect ratio decreases, the rate of the penetration process increases significantly due to reduced resistance from gravity associated with the smaller volume of fluid in the channel. It is seen that the equilibrium penetration depth increases from 90 to 220 when γ decreases from 0.5 to 0.005. For the entire range of γ , the comparison between the analytical and the numerical solutions demonstrates good agreement.

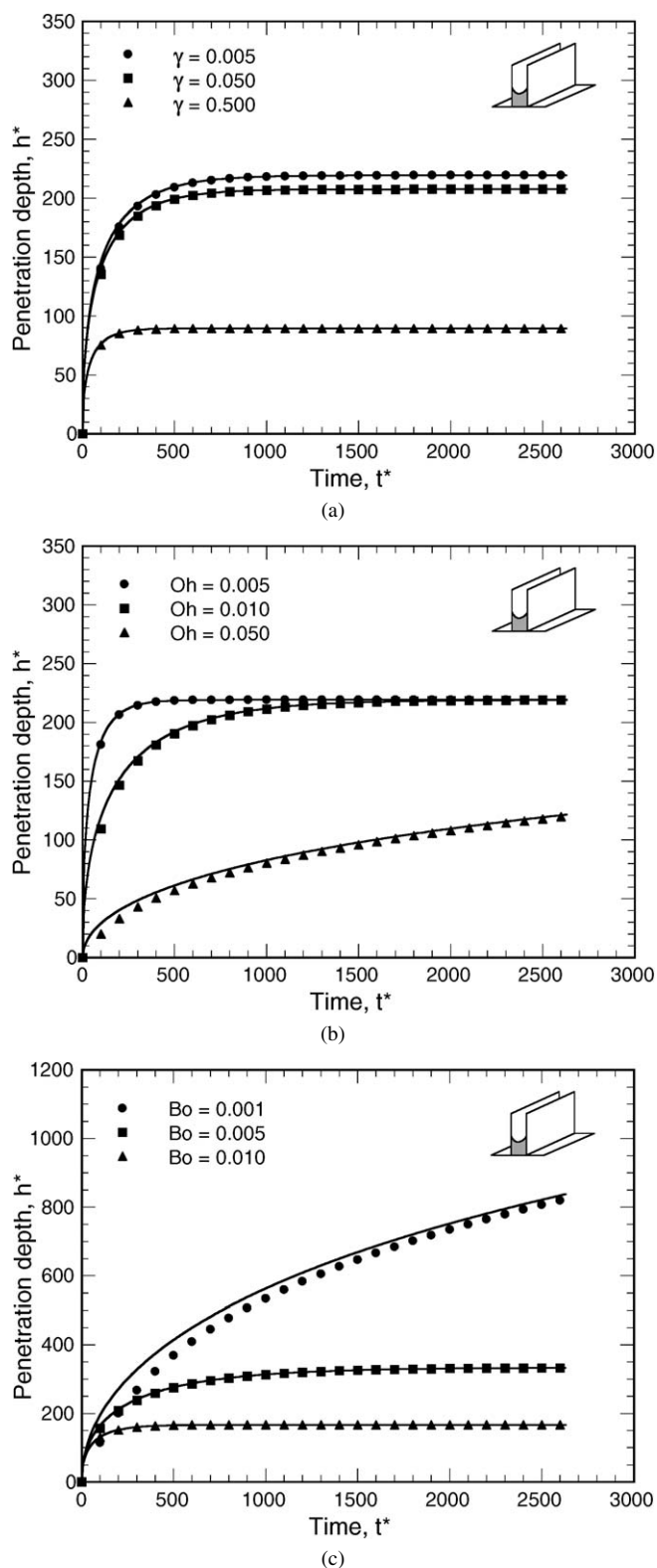


Fig. 3. Penetration depth as a function of time for different (a) aspect ratio, γ , (b) Ohnesorge number, Oh , and (c) Bond number, Bo . The default values of parameters are: (a) $Oh = 0.0075$, $Bo = 0.0076$, (b) $\gamma = 0.006$, $Bo = 0.0076$, and (c) $Oh = 0.0075$, $\gamma = 0.006$.

The effects of Ohnesorge number (Oh) and Bond number (Bo) on the penetration process are shown in Figs. 3b and 3c, respectively, with the corresponding parameter combinations

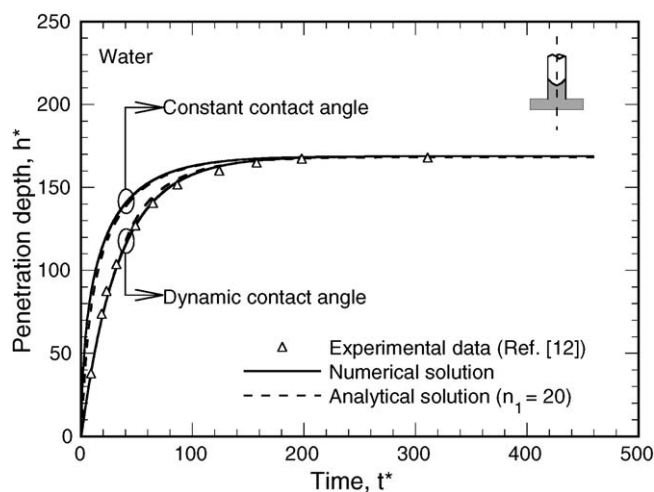


Fig. 4. Penetration depth as a function of time for the capillary flow of water in a vertical tube.

indicated in the figure caption. Since the Ohnesorge number is defined as the ratio of viscous force (resistance to flow) to surface tension (driving the flow), the rate of capillary rise decreases with increasing Ohnesorge number due to increased viscous resistance relative to the driving capillary force. It is seen that the equilibrium penetration depth does not change with the Ohnesorge number (h^* for the case of $Oh = 0.05$ approaches the same equilibrium value as the other two cases in Fig. 3b when the time increases outside the range of the plot). Note that the equilibrium state is established via the balance between capillary force and the gravity force. Since the Bond number is kept constant in Fig. 3b, changing the Ohnesorge number essentially reflects a change in the viscous force, which does not play a role in determining the equilibrium penetration depth. However, the viscous force affects the rate at which the equilibrium is reached, in that the rise is faster with decreasing viscosity, and in turn, the Ohnesorge number, as seen in Fig. 3b. Fig. 3c shows the effect of the Bond number, which is the ratio between gravity to the surface tension. For a fixed time t^* , the penetration depth increases monotonically with decreasing Bond number, owing to reduced resistance from gravity. The results in Fig. 3c suggest that the penetration depth increases as the Bond number decreases, which provides the trend in capillary flows under conditions approaching microgravity. Again, the analytical solutions in Figs. 3b and 3c demonstrate excellent agreement with the corresponding numerical computations.

The results presented so far pertain to capillary flows with constant contact angle, while the cases for dynamic contact angle form the focus of the discussion in the remainder of the section. The flow penetration with time for water in a capillary tube is shown in Fig. 4, where the symbols denote experimental data from Hamraoui et al. [12], and the solid and dashed lines represent the numerical and analytical predictions, respectively. For the combination of water in a glass tube, the parameter M^* in Eq. (5) assumes a value of 38,470, which is obtained by fitting the numerical results with the experimental data. To illustrate the effect of dynamic contact angle, the predictions using constant equilibrium contact angle are also included for com-

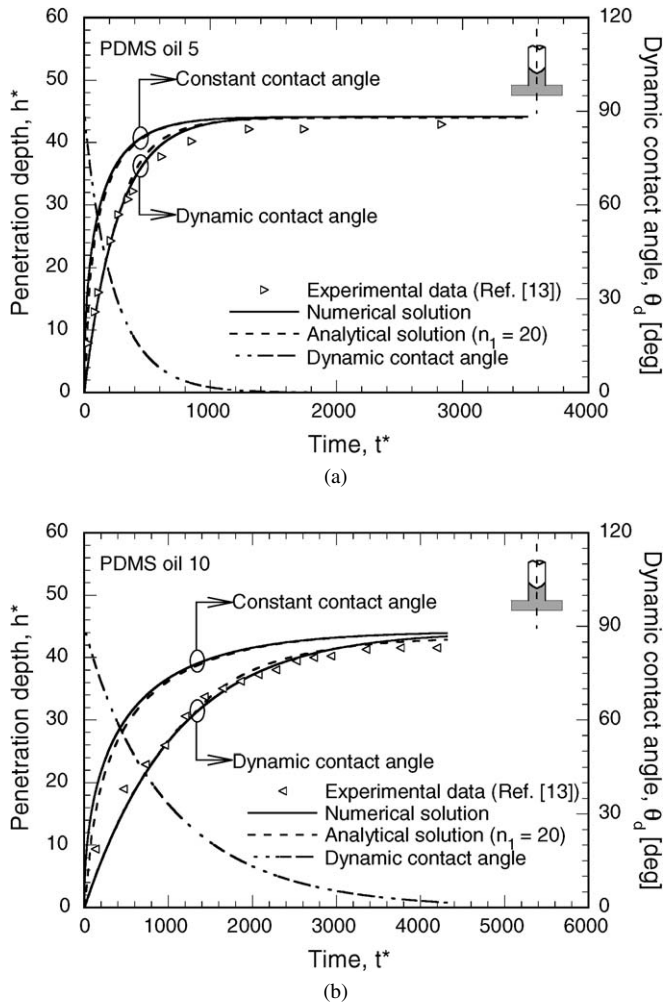


Fig. 5. Penetration depth as a function of time for the capillary flows of (a) PDMS oil 5 and (b) PDMS oil 10 in a vertical tube.

parison. Recall that the analytical solution for dynamic contact angle is obtained by dividing the time space into several intervals, and using Eq. (20) with an average value of contact angle in each time interval. Since a small change of $\cos \theta_d$ in each time interval is desirable for numerical accuracy in using Eq. (20), the temporal space is nonevenly divided such that each interval Δt_i corresponds to the same change in the value of $\cos \theta_d$. In this study, the $\cos \theta_d$ space is divided into 10 equal intervals between $\cos 90^\circ$ (starting value of θ_d at time $t^* = 0$) and $\cos \theta_e$, and the corresponding Δt^* was determined for each interval from a plot of $\cos \theta_d$ with time using Eq. (5). A value of at least 10 for the number of intervals was found to yield convergence of the analytical results to within 1%, based on which the number of intervals is selected to be 10. It is seen that the predictions adopting the constant equilibrium contact angle, θ_e in Eq. (5), deviate significantly from the experimental data, especially in the initial stages of the rise, while the analytical and numerical results using dynamic contact angle compare well with the experimental measurements. The adoption of constant contact angle overpredicts the rate of capillary rise, owing to the larger capillary driving force corresponding to the equilibrium contact angle during the initial stages of the process.

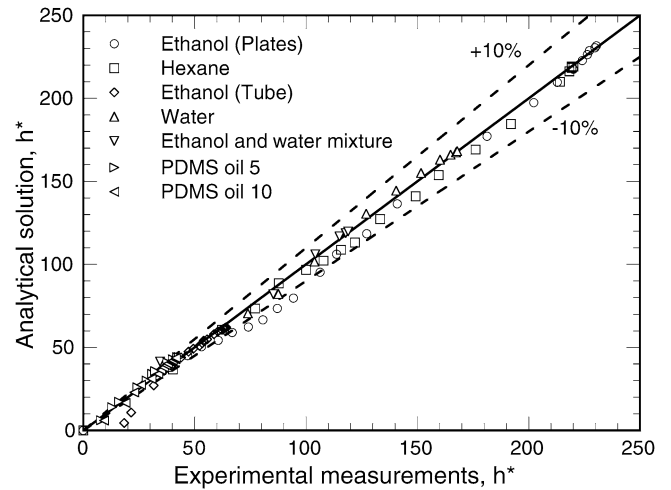


Fig. 6. Summary comparison of the analytical solution with experimental data on the capillary penetration process for all the geometries and fluids considered.

Figs. 5a and 5b show the capillary rise process for PDMS oil 5 and PDMS oil 10, respectively, in a capillary tube of radius $r_0 = 0.315$ mm, and the presentation format follows that in Fig. 4. The values of the empirical parameter M^* are also obtained by fitting the numerical results with the experimental data, which are 3679 for PDMS oil 10, and 4086 for PDMS oil 5. Since the viscosity of PDMS oil 10 is twice as that of PDMS oil 5 while the other properties of the two fluids assume similar values (see Table 2), the rate of penetration in Fig. 5b is much slower than that in Fig. 5a, owing to the larger viscous resistance for PDMS oil 10. Note again that the calculations using constant contact angle overpredict the penetration rate, whereas accounting for the dynamic contact angle yields a closer correspondence with experimental data for both fluids. In the same figures, the evolutions of the dynamic contact angle are also presented. For both of the fluids, the dynamic contact angles start with a value of 90° at the initial time, and gradually decrease to the reported equilibrium value, 0° [13]. The relaxation time for PDMS oil 10 to achieve θ_e is seen to be much longer than that for PDMS oil 5. Since no experimental measurement of the dynamic contact angle is available in the literature for the particular fluid/surface combinations in Fig. 5, a validation of the predicted variations of the dynamic contact angle was not possible.

The results presented in this section are summarized in Fig. 6 where the values of penetration depth measured experimentally are plotted with respect to those obtained from the analytical solution. The diagonal line in the plot corresponds to the line of exact agreement and the dashed lines denote the 10% error bands. Of the total number of 110 data points in the figure, 85.5% are within the $\pm 10\%$ error bands, which demonstrates the validation of the current theoretical analysis over a wide range of fluids and capillary geometries.

The general analytical model developed in this study unifies the studies over the last several decades and may be used to replace the numerical models for various applications of capillary-driven flows. The validation of the analytical solution with the experimental data from various literature sources and

for a wide range of fluids demonstrates the generalized applicability of the theoretical treatment.

5. Conclusions

The various differential equations for the capillary flows in the literature are generalized into a unified nonlinear second-order differential equation which includes the effects of the entrance loss, the inertial force, and the dynamic contact angle. For the capillary flows in vertical parallel plates and tubes, an analytical solution to the general differential equation is obtained by using a double Dirichlet series. The analytical results show a good agreement with numerical solution and the experimental data for a wide range of fluids and capillary geometries reported in the literature, which demonstrates that the analytical model provides a simple and unified approach to predict the evolution of the penetration depth.

Acknowledgment

The work reported is funded in part by the National Science Foundation through Grant No. CTS-0522933. The authors gratefully acknowledge the support.

References

- [1] B.V. Zhmud, R. Tiberg, K. Hallstensson, *J. Colloid Interface Sci.* 228 (2000) 263.
- [2] M. Dreyer, A. Delgado, H.J. Rath, *Micrograv. Sci. Technol.* 4 (1993) 203.
- [3] H.J. Barraza, S. Kunapuli, E.A. O'Rear, *J. Phys. Chem. B* 106 (2002) 4979.
- [4] E.W. Washburn, *Phys. Rev.* 17 (1921) 273.
- [5] P. Raiskinmaki, A.S. Manesh, A. Jasberg, A. Kaponen, J. Merikoski, J. Timonen, *J. Stat. Phys.* 107 (2002) 143.
- [6] A.A. Duarte, D.E. Strier, D.H. Zanette, *Am. J. Phys.* 64 (1996) 413.
- [7] S. Levine, P. Reed, E.J. Watson, in: M. Kerker (Ed.), *Colloid and Interface Science*, vol. III: Adsorption, Catalysis, Solid Surfaces, Wetting, Surface Tension, and Water, Academic Press, New York, 1976, p. 403.
- [8] S. Levine, J. Lowndes, E.J. Watson, G. Neale, *J. Colloid Interface Sci.* 73 (1980) 136.
- [9] M. Dreyer, A. Delgado, H.J. Rath, *J. Colloid Interface Sci.* 163 (1994) 158.
- [10] A.M. Morales, R. Pitchumani, T.J. Garino, A.K. Gutmann, L.A. Domeier, *J. Am. Ceram. Soc.* 88 (2005) 570.
- [11] V.V. Berezkin, N.V. Churaev, *Colloid J. USSR* 44 (1982) 376.
- [12] A. Hamraoui, K. Thuresson, T. Nylander, Y. Yaminsky, *J. Colloid Interface Sci.* 226 (2000) 199.
- [13] A. Hamraoui, T. Nylander, *J. Colloid Interface Sci.* 250 (2002) 415.
- [14] T.S. Jiang, S.G. Oh, J.C. Slattery, *J. Colloid Interface Sci.* 69 (1979) 74.
- [15] P. Joos, P.V. Remoortere, M. Bracke, *J. Colloid Interface Sci.* 136 (1990) 189.
- [16] S. Sciffer, *Chem. Eng. Sci.* 55 (2000) 5933–5936.
- [17] S. Newman, *J. Colloid Interface Sci.* 26 (1968) 209.
- [18] W.E. Brittin, *J. Appl. Phys.* 17 (1946) 37.